The 8th European Congress on Computational Methods in Applied Sciences and Engineering
ECCOMAS Congress 2022
5-–9 June 2022, Oslo, Norway

A FLUID-STRUCTURE INTERACTION STUDY OF HEMODYNAMICS IN ARTERIAL BYPASS-GRAFT ANASTOMOSES

Georgios Bletsos[1], Lars Radtke[2], Alexander Düster[2] and Thomas Rung[1]

[1] Institute for Fluid Dynamics and Ship Theory
Hamburg University of Technology (TUHH)
Am Schwarzenberg-Campus 4, 21073 Hamburg, Germany
e-mail: george.bletsos@tuhh.de, www.tuhh.de/fds

[2] Numerical Structural Analysis with Application in Ship Technology
Hamburg University of Technology (TUHH)
Am Schwarzenberg-Campus 4, 21073 Hamburg, Germany
email: lars.radtke@tuhh.de, www2.tuhh.de/skf

Key words: Arterial Bypass-Graft, Hemodynamics, FSI, CFD

Abstract. This paper reports on numerical experiments on arterial bypass-graft anastomoses. Bypass-grafts are oftentimes used in surgical procedures to divert blood around narrowed or occluded parts of an artery. The diverted blood flow is crucial to the success of the operation as it may lead to undesirable peculiarities that can result to a renewed occlusion in the distal connection of the graft. However, an a priori prediction of detrimental hemodynamic aspects due to undesirable flow properties is difficult to perform in vitro or in vivo conditions. To this end, this work targets to enhance our understanding of harming mechanisms through in silico experiments using computational fluid dynamics (CFD) and fluid-structure interaction (FSI) simulations. The latter are realized through a partitioned coupled approach which is verified for a 2D benchmark case against literature-reported results. Finally, we present numerical results on grafts with different cuff sizes. Wall shear stress (WSS), oscillatory shear index (OSI) and hemolysis are monitored and compared in the context of either rigid or elastic walls and cuff sizes. Special interest is given to the prediction of hemolysis induction which is often not considered in such studies. We show that wall elasticity is the key parameter in terms of WSS prediction while cuff size mainly affects the estimation of OSI.

1 INTRODUCTION

Cardiovascular diseases (CVDs) are the leading global cause of death. An estimated 17.9 million people died from CVDs in 2019, corresponding to 32% of all global deaths [1]. Atherosclerosis is considered to be the prevailing CVD which leads to artery failure due to the formation of plaque. An extensive build-up of plaque can lead to occluded vessels, resulting in narrowed regions (stenoses) where blood flow is restricted. While plaque formation and growth is a process that takes place over time due to systemic risk factors such as smoking, unhealthy diet and low activity, it is also possible for plaque segments to break off and cause a complete occlusion

to smaller, distal vessels [2]. If possible, treatment of stenoses is done using minimal invasive techniques such as prescription medications or, for more severe cases, stent placement. However, if an artery is impaired to such an extent that the functionality of distal organs can no longer be ensured, an open surgery may be advised in order to implant a bypass-graft. The success of the surgery and the implanted graft has been shown to strongly depend on the resulting hemodynamics [3]. In particular, the wall shear stress (WSS) and oscillatory shear index (OSI) have been found to play a significant role in the success of the treatment after the implantation of the prosthetic graft [4].

While the direct success of the operation relies, in large, to the aforementioned factors, the unnatural flow patterns that might develop can indirectly also damage the blood itself. Such a phenomenon is called mechanical hemolysis and refers to the damage of red blood cells due to excessively high stresses. Hemolysis has been the focus of extensive studies in regards to biomedical machinery [5], however, it is usually not considered in studies of arterial bypass-graft anastomoses due to its indirect involvement in the success of the post-operation treatment. An a priori prediction of the aforementioned quantities would thus prove beneficial to the surgical procedure. Such predictions are inevitably difficult to perform both in vitro, e.g. in the laboratory, and in vivo, i.e. on a living patient, conditions. Therefore, in silico experiments, i.e. computational simulations, have seen a large appeal in the past years due to the ever-growing advances in computational science but also due to being able to overcome restrictions arising in vivo or in vitro experimental conditions [6]. In this paper, we employ computational methods to numerically investigate different influences on the hemodynamics of idealized bypass grafts. In specific, we consider a set of simulations that target to investigate the effect of rigid compared to elastic vessel walls and cuff sizes on the resulting hemodynamics. Our interest is confined to the aforementioned two factors based on their relevance to the resulting flow patterns, as shown in [7, 8].

The remainder of this paper is organized as follows: Section 2 outlines the methodological aspects employed to produce the computational simulations and results. In Section 3 we verify the coupling between the fluid and structural solver on a 2D benchmark case. Subsequently, the investigated idealized bypass graft cases are presented and results of our numerical experiments are shown in Section 4. The paper closes with conclusions and outlines further research in Section 5.

Within this publication, Einstein's summation convention is used for repeated lower-case Latin subscripts. Vectors and tensors are defined with reference to Cartesian coordinates.

2 METHODOLOGY

This section outlines the overall numerical methodology. We briefly summarize the formulation of the fluid flow problem, including hemolysis prediction modeling. The formulation is distinguished based on whether rigid walls are considered, thus computational fluid dynamics (CFD) simulations are employed, or compliant walls, which are modeled through coupled fluid-structure interaction (FSI) simulations. To this end, the structural problem is also recapitulated. Numerical aspects for the solution of each subproblem are discussed and a brief overview of the coupling approach is presented. The section closes with a presentation of the hemodynamic quantities of interest.

2.1 Fluid problem

Blood is modeled as an incompressible, Newtonian fluid. All investigated flow scenarios are assumed to be transient and laminar, with a maximum estimated Reynolds number of Re=600. If the surrounding walls of the graft and the impaired vessel are considered to be rigid then the domain occupied by the fluid is time independent and we denote it by Ω_f. The flow follows from the incompressible Navier-Stokes (NS) equations for the conservation of volume and momentum, viz.

$$R^p = \frac{\partial u_j}{\partial x_j} = 0 \qquad \text{in} \quad \Omega_f \tag{1}$$

$$R^u_i = \frac{\partial u_i}{\partial t} + u_j \frac{\partial u_i}{\partial x_j} - \frac{\partial}{\partial x_j}\left[2\nu^f S_{ij} - \bar{p}\delta_{ij}\right] = 0 \qquad \text{in} \quad \Omega_f. \tag{2}$$

In the case of compliant walls, the fluid domain changes in time and we refer to it as Ω^τ_f. In this case, the continuity equation (1) holds the same in Ω^τ_f while the momentum equations are reformulated so that the domain or grid velocity is considered in the convective term

$$\bar{R}^u_i = \frac{\partial u_i}{\partial t} + (u - u^m)_j \frac{\partial u_i}{\partial x_j} - \frac{\partial}{\partial x_j}\left[2\nu^f S_{ij} - \bar{p}\delta_{ij}\right] = 0 \qquad \text{in} \quad \Omega^\tau_f. \tag{3}$$

In the above, u_i, u^m_i and $\bar{p} = \frac{p}{\rho^f}$ refer to the fluid velocity, domain velocity and specific pressure, respectively. The fluid kinematic viscosity is denoted by ν^f, and density by ρ^f. The components of the strain-rate tensor are denoted by $S_{ij} = 0.5(\partial u_i/\partial x_j + \partial u_j/\partial x_i)$ and δ_{ij} refers to Kronecker delta components.

In the scope of this work, hemolysis estimation is of interest. To this extent, we employ a typical hemolysis prediction model which is one-way coupled to the CFD solver [5, 9]. The one-way coupling implies that the model receives information from the NS equations with no retro-action to them. In a CFD simulation we, thus, additionally target at the solution of

$$R^H = \frac{\partial H_L}{\partial t} + u_j \frac{\partial H_L}{\partial x_j} - C^{\frac{1}{\beta}} \bar{\tau}^{\frac{\alpha}{\beta}} (1 - H_L) = 0 \qquad \text{in} \quad \Omega_f, \tag{4}$$

while for an FSI, one obtains

$$\bar{R}^H = \frac{\partial H_L}{\partial t} + (u - u^m)_j \frac{\partial H_L}{\partial x_j} - C^{\frac{1}{\beta}} \bar{\tau}^{\frac{\alpha}{\beta}} (1 - H_L) = 0 \qquad \text{in} \quad \Omega^\tau_f. \tag{5}$$

Here, $H_L = H^{\frac{1}{\beta}}$ where H denotes a measure for the released hemoglobin to the total hemoglobin within the red blood cell. The phenomenon is governed by shear stresses and $\bar{\tau}$ is used as a scalar stress representation, which is based on the second invariant of the stress tensor $\tau_{ij} = 2\mu^f S_{ij}$, where μ^f is the fluid dynamic viscosity. Specifically, $\bar{\tau}$ is computed as

$$\overline{\tau} = \sqrt{-I_{\tau_2}} \qquad \text{with} \qquad I_{\tau_2} = \frac{1}{2}\left[\left(tr(\tau_{ij})\right)^2 - tr(\tau^2_{ij})\right]. \tag{6}$$

The parameters (C, α, β) employed in Eqns. (4, 5), are introduced to fit experimental data. While the choice of this set of parameters has been extensively discussed in the literature, see f.e

[10, 11, 12], we limit our investigations to $(C, \alpha, \beta) = (3.6 \cdot 10^{-7}, 2.416, 0.785)$ as proposed in [10]. Nevertheless, we acknowledge the fact that a different set of employed constants might lead to predictions that differ by almost an order of magnitude, as shown in [9]. An accurate prediction of hemolysis induction is, to a certain extent, beyond the scope of this paper which is confined to an assessment of the relative changes experienced for different experimental configurations.

The fluid problem is closed by a set of boundary conditions applied to the inlet (Γ_{in}), outlet (Γ_{out}) and wall (Γ_w^τ) patches. Here, we make the distinction between elastic (Γ_{if}^τ) and rigid (Γ_{rw}) parts of the wall such that $\Gamma_w^\tau = \Gamma_{if}^\tau \cup \Gamma_{rw}$. The set of boundary conditions employed for all cases considered in this paper is presented in Table 1. The numerical procedure for

Table 1: Boundary conditions for closing the fluid problem. Here, n_j denotes the normal vector to the surface and $\dot{d}_i$ the structural velocity. The third row thus solely refers to FSI considerations. Notations u_i^{in} and $\bar{p}^{out}$ refer to prescribed values for inlet velocity and outlet pressure, respectively.

Boundary Patch	u_i	$\bar{p}$	H_L
Γ_{in}	$u_i = u_i^{in}$	$n_j \frac{\partial \bar{p}}{\partial x_j} = 0$	$H_L = 0$
Γ_{out}	$n_j \frac{\partial u_i}{\partial x_j} = 0$	$\bar{p} = \bar{p}^{out}$	$n_j \frac{\partial H_L}{\partial x_j} = 0$
Γ_{if}^τ	$u_i = \dot{d}_i$	$n_j \frac{\partial \bar{p}}{\partial x_j} = 0$	$n_j \frac{\partial H_L}{\partial x_j} = 0$
Γ_{rw}	$u_i = 0$	$n_j \frac{\partial \bar{p}}{\partial x_j} = 0$	$n_j \frac{\partial H_L}{\partial x_j} = 0$

the solution of the fluid problem is based upon the finite volume method (FVM) employed by FreSCo$^+$ [13]. The segregated algorithm uses a cell-centered, collocated storage arrangement for all transport properties. The implicit numerical approximation is second order accurate in space and first order accurate in time. The pressure–velocity coupling is based on the SIMPLE method and possible parallelization is realized by means of a domain decomposition approach.

2.2 Structural problem

The structural mechanics equations of state follow from the balance of linear momentum described in terms of a reference, undeformed configuration of the structure, that we denote Ω_s^o. Due to the consideration of a reference and a current configuration (Ω_s^τ), in what follows we subscript quantities that refer to the reference configuration with upper-case indices and ones that refer to the current configuration with lower-case. Formally, the equations are

$$R_i^d = \rho^s \frac{\partial^2 d_i}{\partial t^2} - \frac{\partial (F_{iK} \bar{S}_{KJ})}{\partial X_J} - \rho^s b_i = 0 \qquad \text{in} \quad \Omega_s^o, \tag{7}$$

where d_i denotes the structural displacement vector components. The density of the undeformed structure is defined by ρ^s and b_i denotes the vector of body loads. The deformation gradient is defined as $F_{iK} = \frac{\partial x_i}{\partial X_K} = \delta_{iK} + \frac{\partial d_i}{\partial X_K}$ and $\bar{S}_{KJ}$ denotes the second Piola-Kirchhoff stress tensor. The St. Venant-Kirchhoff material model is used such that $\bar{S}_{KJ} = \lambda \delta_{KJ} E_{II} + 2\mu E_{KJ}$. Here, the notation δ_{KJ}, E_{KJ} is used to represent Kronecker delta and Green–Lagrange strain tensor

components, respectively. The Green-Lagrange strain tensor is defined as $E_{KJ} = \frac{1}{2}(F_{iK}F_{iJ} - \delta_{KJ})$ and the Lamé constants λ and μ are related to Young's modulus (E) and Poisson's ratio (ν^s) based on $\lambda = \frac{E\nu^s}{(1+\nu^s)(1-2\nu^s)}$ and $\mu = \frac{E}{2(1+\nu^s)}$. We also note that the balance of mass is fulfilled by construction and yields $\rho^s_\tau = J\rho^s$ for the density of the current configuration with $J = \det(F_{iK})$.

The structural problem is closed by a set of boundary conditions. At ends (Γ_{end}) we set $d_i = 0$ and at the inner wall (Γ_{if}) we prescribe the fluid loads as a traction boundary condition. The outer wall is traction free.

We solve the structural problem using high-order finite elements with integrated Legendre shape functions, see e.g. [14]. The curved element geometry is defined using the blending function method and interpolating the continuous geometry at optimal interpolation points. The discretization in time is done using the Newmark method. For details about the method implemented in the in-house code AdhoC, the reader is referred to [15].

2.3 Coupling

In the cases that FSI simulations are considered, we follow a partitioned solution approach, in which each subproblem and its respective numerical solver are considered as black boxes. This is schematically sketched by consideration of the operator formulation, in which

$$d_i^{n+1} = \mathcal{S}(t_i^{n+1}) \tag{8}$$

denotes the solution of one time step $(n+1)$ of the structural subproblem, which yields displacements d_i^{n+1} given tractions t_i^{n+1}. It is noted, that the aforementioned vectors refer solely to points on the coupling interface Γ^τ_{if}. In a similar manner, the fluid subproblem can be abbreviated as

$$t_i^{n+1} = \mathcal{F}(d_i^{n+1}). \tag{9}$$

In a coupled problem $d_i^{n+1} = \mathcal{S}(\mathcal{F}(d_i^{n+1}))$ and $t_i^{n+1} = \mathcal{F}(\mathcal{S}(t_i^{n+1}))$ must hold. To this extent, the solution of the aforementioned fixed-point equations is realized through accelerated fixed-point iterations for each time step. The complete coupling process is realized through comana [16]. In the cases studied herein, we accelerated the convergence of the coupling iterations using the quasi-Newton least-squares method introduced in [17] resulting to no more than 10 coupling iterations per time step. Convergence of the coupling was monitored based on metrics of the residuals of displacement and traction. A detailed explanation of the coupling procedure applied to cardiovascular FSI can be found in [18].

2.4 Quantities of interest

As discussed in Section 1, this work targets to predict WSS and OSI due to their direct relevance to potential post-operation restenosis as well as hemolysis induction (HI) that might be caused due to unnatural flow patterns. All quantities are computed in the fluid subproblem. Formally, for the estimation of WSS, we compute the vector

$$\tau_k^w = 2\mu^f \Big(S_{kj}n_j - (S_{ij}n_in_j)n_k \Big). \tag{10}$$

We then extract an indicator field in time

$$\tau_k^{max} = \max_{t\in[t^*,t^*+T]} \tau_k^w, \tag{11}$$

from which we can then extract two scalar quantities for each simulation, referring to the spatial minimum or maximum of the temporal maximum (Eqn. (11)) WSS, as

$$\tau^{max,min} = \min_{x\in\Gamma_w^\tau} \|\tau_k^{max}\| \qquad \text{and} \qquad \tau^{max,max} = \max_{x\in\Gamma_w^\tau} \|\tau_k^{max}\|. \tag{12}$$

The quantities computed from Eqns. (12) serve as indicators since both very high and low WSSs are classified as problematic to the desired post-operation recovery. Another crucial indicator, that has been shown to predict the initiation of intimal hyperplasia and thus the offset of a renewed stenosis, is OSI. The computation of OSI follows from

$$\text{OSI} = \frac{1}{2}\Big(1 - \frac{\| \int_{t^*}^{t^*+T} \tau_k^w dt\|}{\int_{t^*}^{t^*+T} \|\tau_k^w\| dt}\Big). \tag{13}$$

As can be easily seen, the value of OSI is bounded in $[0, 0.5]$, where 0.5 indicate the most potentially problematic regions. Equation (13) results in a spatial distribution of OSI for each investigated simulation. In order to enable direct comparisons, we assume a critical region in which we extract the spatial average OSI_{ave}^c.

In order to quantify HI, we first compute the mass-flow-average of hemolysis on the outlet of the computational domain

$$\text{HI} = \frac{\int_{\Gamma_{out}} H\rho^f u_j n_j d\Gamma}{\int_{\Gamma_{out}} \rho^f u_j n_j d\Gamma}. \tag{14}$$

This index is, frequently, employed to quantify HI [9, 5]. However, since all simulations considered herein refer to unsteady flows, we further consider the time averaged HI, computed as

$$\text{TAHI} = \frac{1}{T}\int_{t^*}^{t^*+T} \text{HI} dt. \tag{15}$$

In the above, t^* refers to the start time of the last simulated heartbeat while $T = 0.8$s to approximately one heartbeat.

3 VERIFICATION

This section serves to verify the coupling between the fluid solver (FreSCo$^+$) and the structural solver (AdhoC) through comana. The benchmark problem refers to the well-known 2D lid-driven cavity flow, which is sketched in Fig. 1(a). The employed computational grid for the fluid subproblem consists of 1521 control volumes (CVs). A linear pulsating velocity profile is prescribed on the inlet patch, as shown in Fig. 1(a), with a period of $T = 5$s. The top wall is moving with the maximum velocity of the inlet while the vertical walls are modelled as rigid. The bottom wall is assumed to be deformable. Density and viscosity of the fluid are set to $\rho^f = 1\frac{kg}{m^3}$ and $\mu^f = 0.01$Pa.s, respectively, resulting to an average (in time) $Re = 12.5$.

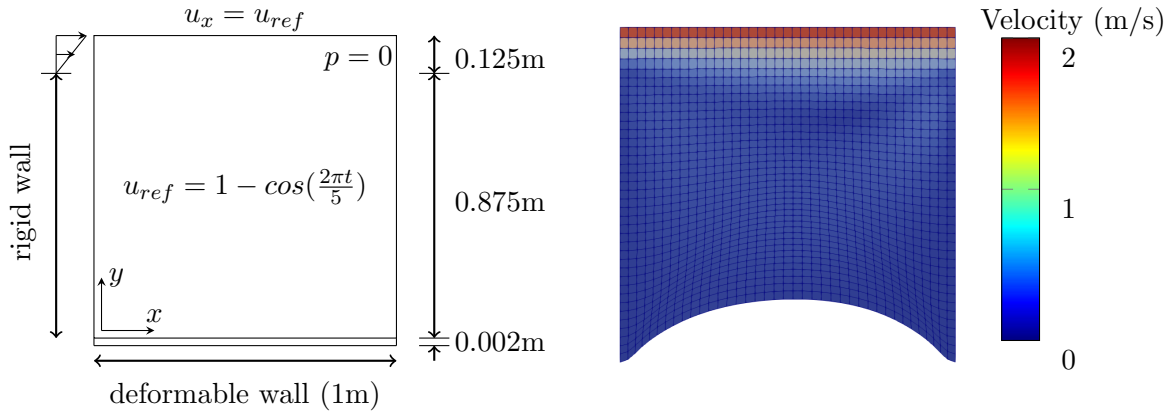

(a) (b)

Figure 1: (a) Sketch of the 2D verification case. (b) Deformed fluid computational mesh at $t = 27.5$s coloured by magnitude of the fluid velocity vector.

For the elastic wall, density and Young's modulus are set to $\rho^s = 500\rho^f$ and $E = 500$Pa, respectively, while Poisson's ratio is set to zero. For its discretization, 16 isoparametric finite elements with quadratic shape functions are used. In Fig. 1(b), we show the deformed fluid mesh at $t = 5.5T$ which sustains a satisfactory level of grid quality. The deformation of the internal nodes of the mesh is realized by means of a Laplacian with a diffusivity inversely proportional to nearest wall distance. We simulate this case for a total of $10T$ and employ a time step $\Delta t = 0.002T$. For verification purposes, we monitor the vertical displacement of the midpoint of the deformable wall and compare it with previously literature-reported results, as shown in Fig. 2. The significant deviations between results shown herein and those in [19] are attributed to a difference in boundary conditions while those with [20] might be caused due to a different time-integration scheme employed in the latter. Nevertheless, the excellent agreement with results in [21] serves to verify the coupling between the fluid and structural solver employed within this work.

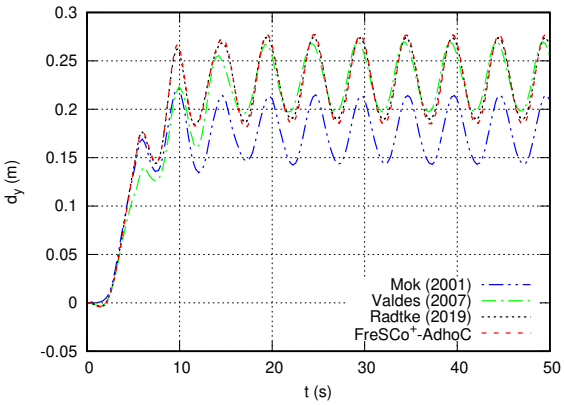

Figure 2: Vertical displacement of deformable's wall midpoint. Mok (2001), Valdes (2007) and Radtke (2019) correspond to results reported in [19, 20, 21], respectively.

4 NUMERICAL EXPERIMENTS

In this section we study 3D idealized arterial bypass-grafts of different cuff sizes considering either rigid or elastic walls. A generalized geometry of the investigated cases is shown in Fig. 3. We consider the top leftmost patch of the geometry to be the exclusive flow inlet. The impaired vessel, on which the graft is implanted to, is modeled as a straight pipe and

considered to be fully occluded, thus the bottom leftmost patch is modeled as a rigid wall. The rightmost patch of the impaired vessel corresponds to the flow outlet. The remaining part of the fluid boundary is modeled as rigid for CFD simulations or elastic for FSI ones. The boundary conditions of the fluid flow are prescribed based on Table 1. In specific, at the inlet we prescribe a Womersley velocity profile based on the periodic volumetric flux shown in Fig. 4. At the outlet, while the prescribed value of pressure is irrelevant for CFD simulations, due to the incompressible nature of the fluid, this is not the case for FSI simulations in which traction is communicated from the fluid solver to the structural one. To this extent, an implicit boundary condition that computes the pressure in terms of the fluid flow, is prescribed at the outlet. This is done through the use of a three-component windkessel model, which can be classified as a zero-dimensional model, viz.

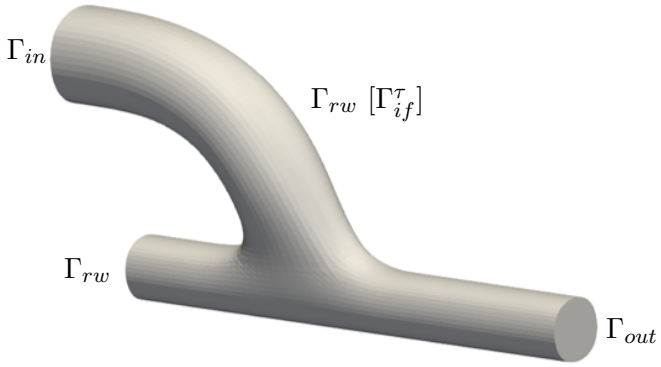

Figure 3: Idealized 3D bypass-graft anastomosis.

$$\left(1+\frac{R_2}{R_1}\right)Q^o + CR_2\frac{dQ^o}{dt} = \frac{p^o}{R_1} + C\frac{dp^o}{dt}. \tag{16}$$

Here, p^o and Q^o denote the desired pressure and flux at the outlet, respectively. Parameters R_1, R_2 and C are selected so that the resulting periodic pressure pulsates between $10-34$ mmHg. The temporal derivatives of flux and pressure are discretized using first-order accurate backward differences and Eqn. (16) is solved for each SIMPLE iteration. Fluid properties are set as such to model blood, with density equal to $\rho^f = 10^3 \frac{kg}{m^3}$ and viscosity $\mu^f = 4 \cdot 10^{-3}$Pa.s. The structure is assumed to be a nearly incompressible, hyperelastic solid with density $\rho^s = \rho^f$, Young's modulus $E = 10^6$Pa and Poisson's ratio $\nu^s = 0.49$.

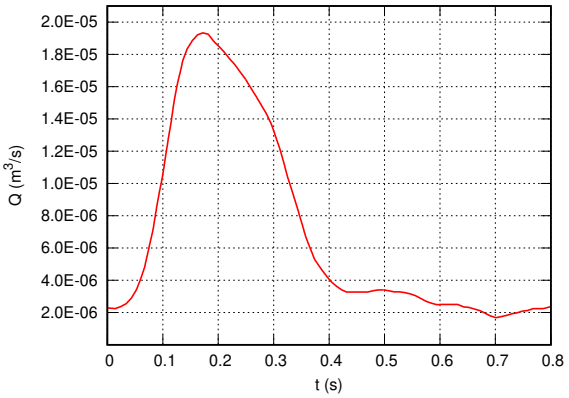

Figure 4: Periodic volumetric flux at the inlet of the idealized bypass-graft anastomosis.

For the numerical solution, we employ a structured hexahedral mesh of approximately 100k CVs for the fluid and a structured hexahedral mesh of 172 elements for the structure.

4.1 Classification of cases

This work considers 3 idealized bypass-graft anastomoses that differ exclusively in the size of the cuff, i.e. connection between the graft and the impaired vessel, as shown in Fig. 5. The circumferential area of the connection changes based on its length on the longitudinal direction with no difference on the in-plane direction (as shown in Fig. 5). For all geometries, CFD and

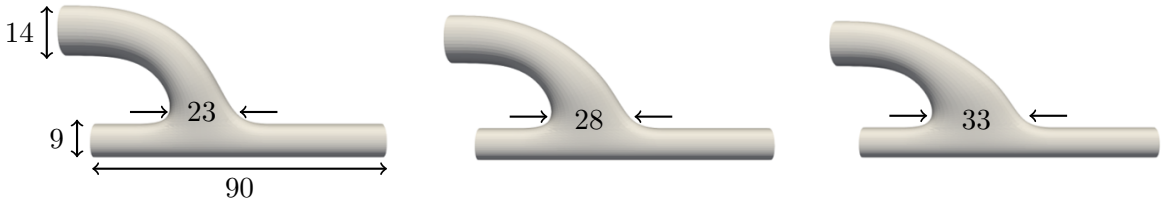

Figure 5: Sketch of the investigated idealized bypass-graft anastomoses. All dimensions shown in [mm]. We refer to each one of them as (left) **Small**, (middle) **Medium** and (right) **Large**.

FSI simulations are realized, resulting to a total of 6 simulations. We refer to each simulation based on the initial letter of the simulation approach and the size of the geometry, e.g. we refer to the case in which a CFD simulation is realized on the medium-sized geometry as *CM*.

4.2 Results

Results of WSS, OSI and HI are collected for all 6 investigated cases. In specific, for each simulation we extract 2 scalar values to characterize WSS, as computed from Eqns. (12), a scalar value for OSI^c_{ave}, based on Eqn. (13) and the time averaged HI as computed from Eqn. (15). As regards the critical region in which OSI^c_{ave} is averaged in, this corresponds to a close neighbourhood of the cuff. For computations herein, we exclude the occluded and distal part of the impaired vessel as well as part of the inlet section of the graft, since values of OSI were found to be trivial in these regions. Heel, toe and bed regions of the anastomoses are included in the computations - the reader is referred to Fig. 3.10 of [21] for specification of the aforementioned terminology. Figure 6 shows the collected results of the investigated cases. As can be seen, the influence of considering compliant walls -which also represent the real world more faithfully- is most significant on the prediction of WSS metrics as well as TAHI. In specific, it is shown that considering rigid instead of elastic walls can lead to a prediction of $\tau^{max,max}$ increased by 51%. Concurrently, $\tau^{max,min}$ is under-predicted by up to 47% in the case of a medium-sized cuffed anastomosis. As for HI, due to the direct relation between the offset of the phenomenon and fluid shear stresses (cf. Eqns. (4,5)) the trend of predictions follow that of $\tau^{max,max}$ with rigid walls simulations over-predicting the investigated quantity to a significant extent. Lastly, our simulations show a negligible influence of wall elasticity on the estimation of OSI^c_{ave}. Overall and in large, we show that neglecting wall elasticity can lead to a higher risk assessment for the post-operation period than what might be realistic.

On the other hand, the investigated OSI metric is found to be most sensitive to different sizes of the cuff. We show that increasing the longitudinal length of the connection between the graft and the impaired vessel by 44% leads to an increase of OSI^c_{ave} by 58%. At the same time, however, we also notice that the aforementioned change in cuff size reduces TAHI by 25%. The contradicting trends of OSI and HI with respect to cuff size is of interest since we would optimally target at the minimization of both. Finally, as regards WSS metrics, the influence of cuff size is shown to be of less importance.

We would also like to note, that the values shown herein should be regarded qualitatively rather than quantitatively. For example, our estimations of TAHI are significantly lower than those in flow scenarios and geometries in which hemolysis is the prime problem, (see i.e. [5, 9]).

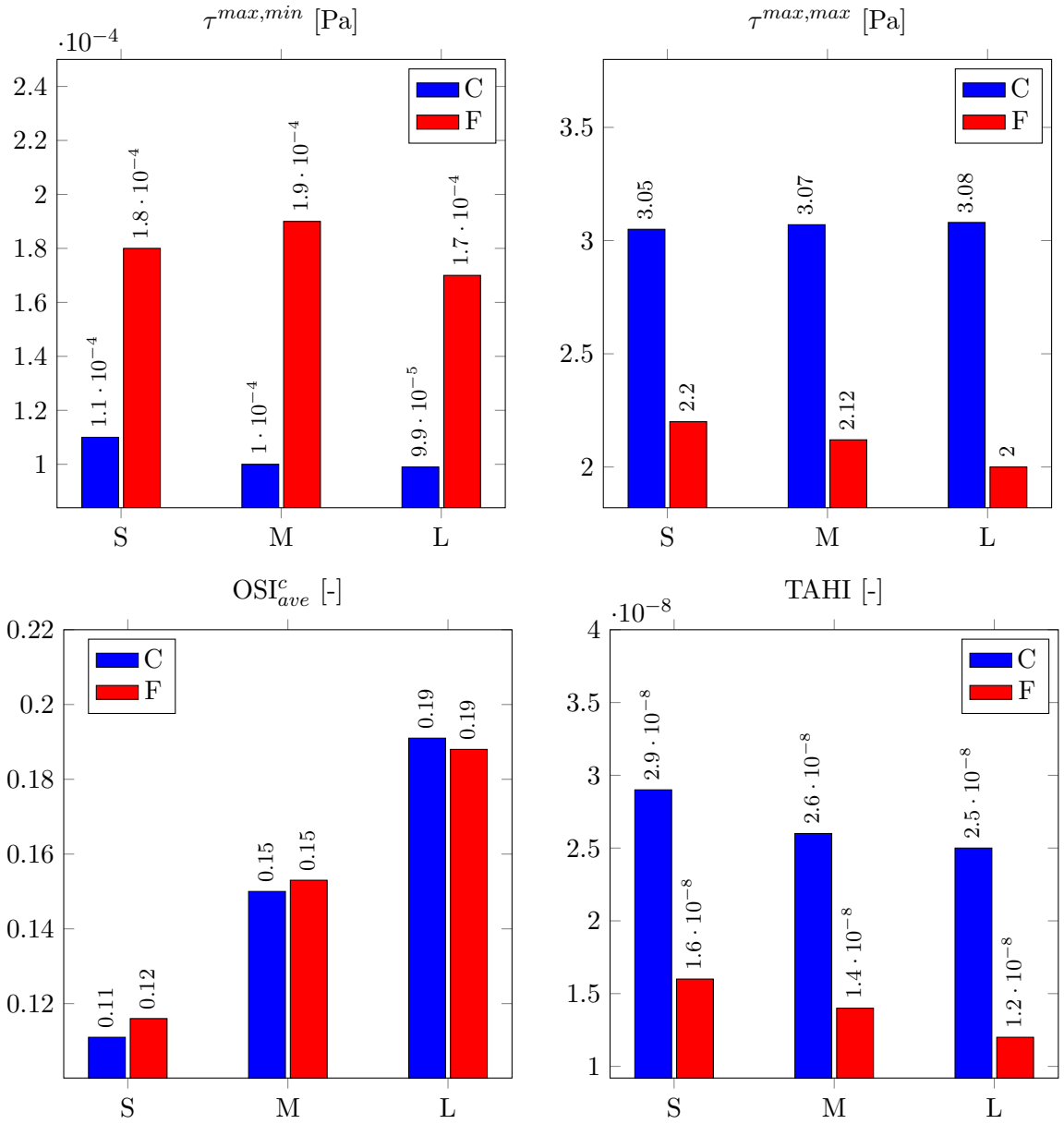

Figure 6: Results for WSS, OSI and HI for the three idealized bypass-graft anastomoses considering rigid or elastic walls. Results obtained from CFD and FSI simulations are presented in blue and red, respectively, while (S,M,L) denote small-,medium- and large-cuffed geometries.

While this might be partially attributed to the selection of hemolysis-related parameters, it is also inherently related to the inflow flux of blood. Due to the stochastic and complicated nature of a physiological blood flow in vivo conditions, it is the authors' belief that in the course of a reasonable time span, the aforementioned values can significantly change. Nevertheless, we believe that the trends presented herein hold under a vast range of physiological conditions.

5 CONCLUSIONS

This paper discusses the influence of rigid compared to elastic vessels as well as cuff sizes on hemodynamic quantities of interest in arterial bypass-graft anastomoses. Rigid wall simulations are realized through the numerical solution of the NS equations augmented by a hemolysis prediction model. To account for compliant walls, the fluid subproblem is coupled to a structural problem through a partitioned scheme. The coupling of the fluid and structural solver is verified on a 2D benchmark. Finally, we apply our methodology in 3 idealized 3D bypass-graft anastomoses of different cuff sizes. It is demonstrated that the wall elasticity can significantly change the prediction of WSS as well as HI, while the shape of the cuff impacts mainly OSI and to a smaller extent HI. The contradicting trends of OSI and HI in terms of cuff size highlight the potential of a formal shape optimization study, in which the two quantities could be casted on a single objective as a weighted sum. Finally, we would like to acknowledge the possibility of considering CFD simulations on geometries which are pre-pressurized, thus displaced to a mean configuration with respect to an FSI one. Future work will target to augment the current study by consideration of different inlet paths, resulting to different inlet velocity profiles, non-Newtonian properties of blood, exercise conditions as well as uncertainties of material properties. Finally, work is currently conducted by the group of authors for the development of an adjoint-based shape optimization method for the minimization of OSI.

ACKNOWLEDGMENTS

The current work is part of the research training group "Simulation-Based Design Optimization of Dynamic Systems Under Uncertainties" (SENSUS) funded by the state of Hamburg within the Landesforschungsförderung under project number LFF-GK11. FSI simulations were performed with resources provided by the North German Supercomputing Alliance (HLRN). This support is gratefully acknowledged by the authors.

REFERENCES

[1] World Health Organization (WHO). *Fact sheets: Cardiovascular diseases*. (2021). URL: https://www.who.int/news-room/fact-sheets/detail/cardiovascular-diseases-(cvds) (visited on 30/05/2022).

[2] Badimon, L. and Vilahur, G. Thrombosis formation on atherosclerotic lesions and plaque rupture. *J. Intern. Med.* (2014) **276**(6):618–632.

[3] Chiu, J. J. and Chien, S. Effects of disturbed flow on vascular endothelium: pathophysiological basis and clinical perspectives. *Physiol Rev.* (2011) **91**(1):327–387.

[4] Ghista, D. N. and Kabinejadian, F. Coronary artery bypass grafting hemodynamics and anastomosis design: a biomedical engineering review. *Biomed Eng Online* (2013) **12**:129.

[5] Yu, H., Engel, S., Janiga, G. and Thévenin, D. A review of hemolysis prediction models for computational fluid dynamics. *Artif. Organs* (2017) **41**(7):603–621.

[6] Owida, A. A., Do, H. and Morsi, Y. S. Numerical analysis of coronary artery bypass grafts: An over view. *Comput Methods Programs Biomed* (2012) **108**(2):689–705.

[7] Bazilevs, Y., Hsu, M.-C., Benson, D. J. et al. Computational fluid–structure interaction: methods and application to a total cavopulmonary connection. *Comput. Mech.* (2009) **45**:77–89.

[8] Rückert, R. I. Experimentelle und klinische Untersuchungen zur Optimierung der Hämodynamik in termino-laterial Prothesenbypass-Anastomosen. Postdoctoral thesis *Humboldt-Universität zu Berlin* (2001).

[9] Bletsos, G., Kühl, N. and Rung, T. Adjoint-based shape optimization for the minimization of flow-induced hemolysis in biomedical applications. *Eng. Appl. Comput. Fluid Mech.* (2021) **15**(1):1095–1112.

[10] Giersiepen, M., Wurzinger, L. J., Opitz, R. and Reul, H. Estimation of shear stress-related blood damage in heart valve prostheses - in vitro comparison of 25 aortic valves. *Int. J. Artif. Organs.* (1990) **13**(5):300–306.

[11] Heuser, G. and Opitz, R. A Couette viscometer for short time shearing of blood. *Biorheology* (1980) **17**:17–24.

[12] Zhang, T., Taskin, M. E. and Fang, H. B. Study of flow-induced hemolysis using novel Couette-type blood-shearing devices. *Artif. Organs* (2011) **35**(12):1180–1186.

[13] Rung, T., Wöckner, K. et al. Challenges and perspectives for maritime CFD applications. *Jahrbuch Der Schiffbautechnischen Gesellschaf* (2009) **103**:127–139.

[14] Szabó, B. A. and Babuška, I. *Finite element analysis.* John Wiley & Sons, (1991).

[15] Radtke, L., König, M. and Düster, A. The influence of geometric imperfections in cardiovascular FSI simulations. *Comput. Math. with Appl.* (2017) **74**(7):1675–1689.

[16] König, M., Radtke, L. and Düster, A. A flexible C++ framework for the partitioned solution of strongly coupled multifield problems. *Comput. Math. with Appl.* (2016) **72**(7):1764–1789.

[17] Degroote, J., Bathe, K. J. and Vierendeels, J. Performance of a new partitioned procedure versus a monolithic procedure in fluid-structure interaction. *Comput. Struct.* (2009) **87**(11):793–801.

[18] Radtke, L., Larena-Avellaneda, A., Debus, E. S. and Düster, A. Convergence acceleration for partitioned simulations of the fluid-structure interaction in arteries. *Comput. Mech.* (2016) **57**:901–920.

[19] Mok, D. P. Partitionierte Lösungsansätze in der Strukturdynamik und der Fluid-Struktur-Interaktion. *PhD Thesis* (2001).

[20] Valdés, J. G. Nonlinear Analysis of Orthotropic Membrane and Shell Structures Including Fluid-Structure Interaction. *PhD Thesis* (2007).

[21] Radtke, L. A partitioned solution approach for fluid-structure interaction problems in the arterial system. *PhD Thesis* (2019).